nature climate change

LETTERS

PUBLISHED ONLINE: 19 MAY 2013 | DOI: 10.1038/NCLIMATE1907

Changes in rainfall seasonality in the tropics

Xue Feng[1], Amilcare Porporato[1,2]* and Ignacio Rodriguez-Iturbe[3]

Climate change has altered not only the overall magnitude of rainfall but also its seasonal distribution and interannual variability worldwide[1–3]. Such changes in the rainfall regimes will be most keenly felt in arid and semiarid regions[4], where water availability and timing are key factors controlling biogeochemical cycles[5], primary productivity[6,7], and the phenology of growth and reproduction[8–10], while also regulating agricultural production[11]. Nevertheless, a comprehensive framework to understand the complex seasonal rainfall regimes across multiple timescales is still lacking. Here, we formulate a global measure of seasonality, which captures the effects of both magnitude and concentration of the rainy season, and use it to identify regions across the tropics with highly seasonal rainfall regimes. By further decomposing rainfall seasonality into its magnitude, timing and duration components, we find increases in the interannual variability of seasonality over many parts of the dry tropics, implying increasing uncertainty in the intensity, arrival and duration of seasonal rainfall over the past century. We show that such increases in rainfall variability were accompanied by shifts in its seasonal magnitude, timing and duration, thus underscoring the importance of analysing seasonal rainfall regimes in a context that is most relevant to local ecological and social processes.

Life in seasonal biomes is uniquely challenged by the requirement to cope with the uncertain arrival and duration of adverse conditions and to flourish during favourable conditions. In the tropics, seasonal rainfall has distinctly shaped a mosaic of highly diverse ecosystems—from the tropical dry forests to open woodland forests to savannas[8]—that support species with a variety of adaptive strategies. Most of these ecosystems are extremely sensitive not only to the annual rainfall amount but also to other aspects of seasonal rainfall—such as the arrival of rain at the beginning of the wet season, which determines the timing of important life stages such as leaf flushing and flowering; and the wet season length, which contributes to the timing of leaf fall and thus the total transpiration period[12–14]. The same rainfall seasonality, with its associated drought and flood risks, also poses huge challenges to local populations, making agricultural efforts and sustainable management of soil and water resources more difficult[11,15].

Seasonality in the rainfall regime can be associated with the magnitude, timing and duration of the wet/dry seasons and is often quantified by analysing the monthly rainfall climatology[16]. On one hand, the literature has produced a confounding number of metrics—such as the relative lengths and rainfall amounts of the wet and dry seasons and the arrival dates of the 25th and 75th percentile rainfall[17,18]—which are often tailored for specific locations and research purposes but rarely applied systematically over larger regions. Other studies, when juxtaposing different locations, tend to focus on their differences in rainfall amount[2] while neglecting its temporal distribution. Thus, as a starting point for a global analysis of seasonal rainfall regimes, we propose a generalized seasonality index that consolidates the rainfall amount with its annual distribution. To isolate patterns stemming from seasonal rainfall variability from those related to temperature variability, we take a section around the Equator between 20° S and 20° N and compute seasonality indices using monthly rainfall data from 2,715 stations in the Global Historical Climatology Network[19].

For each station, we first compute its long-term mean monthly rainfall and then normalize by the mean annual rainfall ($\bar{R}$), resulting in a discrete probability distribution of monthly rainfall ($\bar{p}_m$) for each month m (see Methods). The relative entropy[20] of $\bar{p}_m$ (denoted by $\bar{D}$) with respect to the uniform distribution ($q_m = 1/12$ for all m) quantifies the extent of rainfall concentration in the wet season and can be found using $\bar{D} = \sum_{m=1}^{12} \bar{p}_m \log_2(\bar{p}_m/q_m)$. The dimensionless long-term seasonality index $\bar{S}$ for each station is then constructed by combining multiplicatively its mean annual rainfall, normalized by the observed maximum mean annual rainfall in the data set, $\bar{R}_{\max}$, with its relative entropy, that is,

$$\bar{S} = \bar{D} \cdot \frac{\bar{R}}{\bar{R}_{\max}} \tag{1}$$

such that $\bar{S}$ is 0 when $\bar{R}$ is distributed uniformly throughout the year and maximized (at $\log_2 12 = 3.585$) when $\bar{R}_{\max}$ is concentrated in a single month. As shown in Fig. 1, a desert environment such as in Chad has a low seasonality index despite the intermittent nature of its rainfall (high $\bar{D}$) because mean annual rainfall $\bar{R}$ is low. Similarly, in a humid environment such as Papua New Guinea where rainfall is high year round, the seasonality index can nevertheless be diminished by the low contrast between the seasons (low $\bar{D}$). Thus, a low seasonality index can be attributed to a reduction in either the rainfall amount or its relative entropy (Fig. 1).

As mean annual rainfall and relative entropy can be negatively correlated, the highest seasonality indices are found in areas with intermediate levels of mean annual rainfall. These hotspots of rainfall seasonality appear in the northeast region of Brazil, western sub-Saharan and central Africa, northern Australia, and parts of Southeast Asia and Central America (Fig. 1). These findings can be corroborated by replicating the analysis on a gridded data set[21] (Fig. 2; Methods), which also points to central Brazil and parts of Amazonia as seasonality hotspots. Furthermore, trend analysis on yearly time series of seasonality reveals areas that have experienced marked changes in their seasonality from 1930 to 2002 (Fig. 2; Methods) due to a combination of changes in their mean annual rainfall and/or its monthly distribution (Supplementary Fig. S3). In particular, western Africa and central Brazil stand out as highly seasonal regions that have undergone marked decreases in their seasonality due to decreases in their rainfall amounts

[1]Department of Civil and Environmental Engineering, Duke University, North Carolina 27708, USA, [2]Nicholas School of the Environment and Earth Sciences, Duke University, North Carolina 27708, USA, [3]Department of Civil and Environmental Engineering, Princeton University, New Jersey 08544, USA. *e-mail: amilcare.porporato@duke.edu

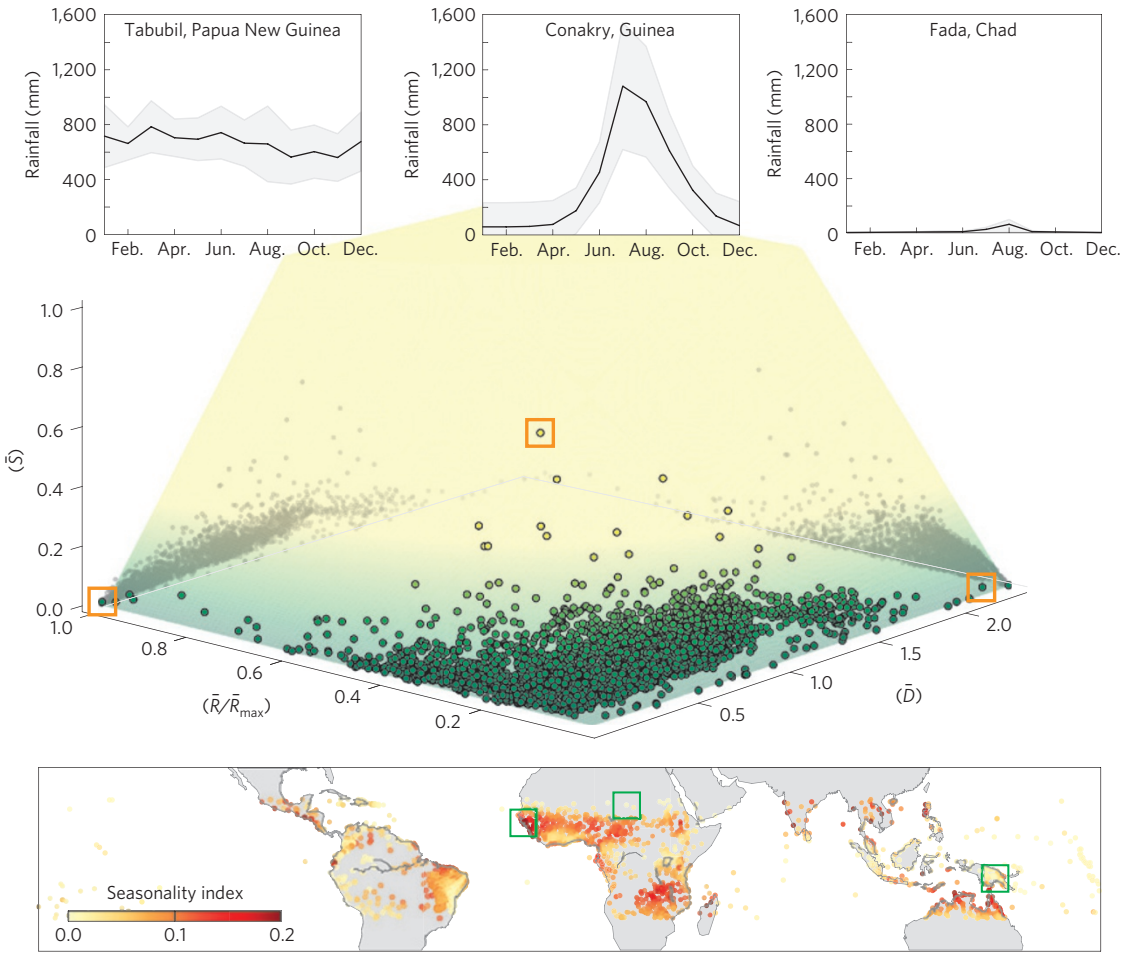

Figure 1 | Seasonality index in the tropics. Top panel, the seasonality index ($\bar{S}$) is shown for stations in the GHCN-Monthly data set as a function of normalized mean annual rainfall ($\bar{R}/\bar{R}_{max}$) and relative entropy ($\bar{D}$). The insets show qualitative differences in the monthly rainfall distribution between locations with high $\bar{R}$, high $\bar{D}$ and high $\bar{S}$, indicated by orange boxes. Green shading indicates low seasonality index, lightening to yellow as $\bar{S}$ increases. Bottom panel, the seasonality indices for all the stations in the top panel are shown, with the locations of the inset plots outlined in green.

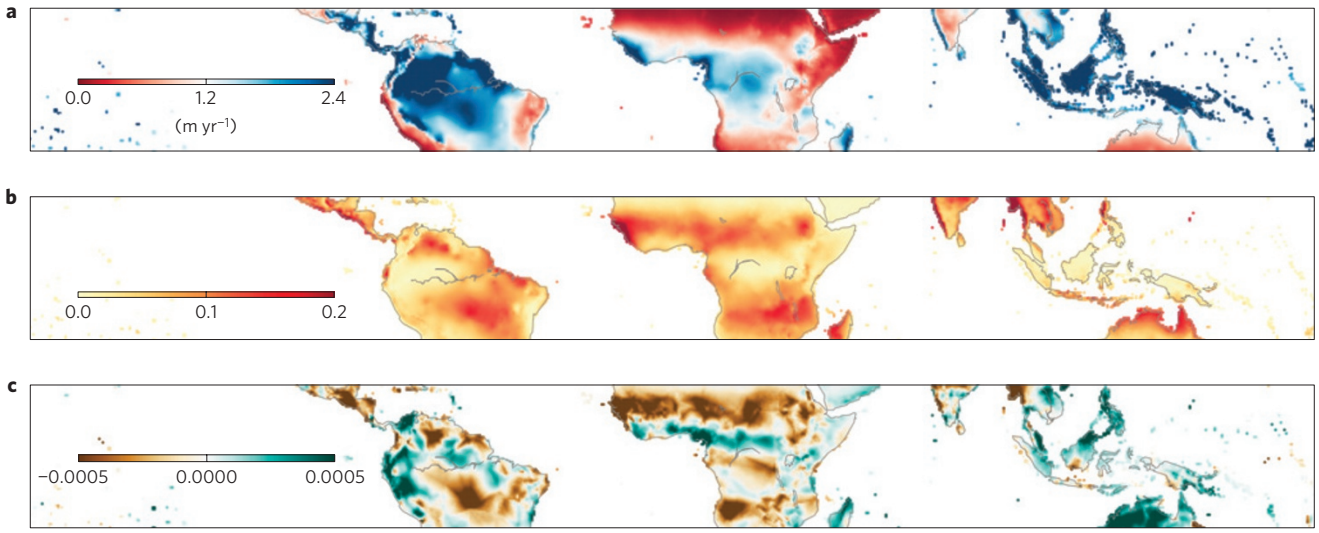

Figure 2 | Mean annual rainfall, seasonality indices and their trends. a–c, The mean annual rainfall (**a**), seasonality index (**b**) and changes in the seasonality index per year (**c**) in the tropics, calculated over the time period 1930–2002 using gridded data from the CRU TS 2.1 data set.

(western Africa) and distribution (central Brazil), whereas the increase in seasonality in northwestern Australia can be traced to large increases in the rainfall total. Furthermore, changes in the rainfall regimes on continental Africa have notably resulted in latitudinal bands alternating between increases and decreases in their seasonality (Fig. 2).

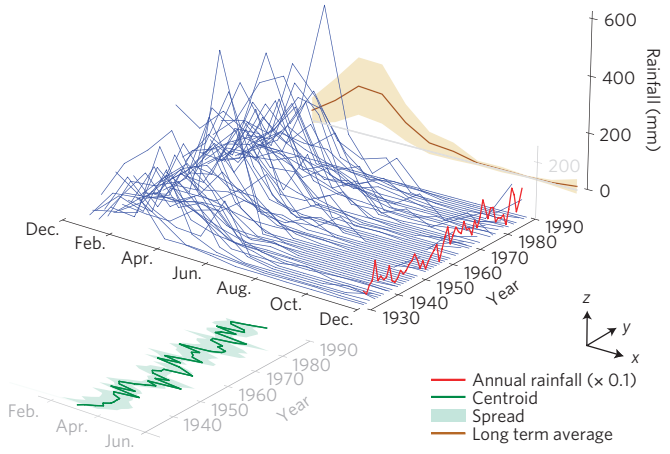

Figure 3 | Decomposition of a monthly rainfall series. The monthly rainfall series for Parau, Brazil (5.78° S, 37.1° W) span 60 years (1930–1990), with each year's distribution plotted next to each other (thin blue lines). The long-term average monthly rainfall distribution is shown in brown, with the beige area spanning the standard deviation. The projection for the annual rainfall is indicated in red. The centroid (dark green line) and the spread (light green area) are also shown.

We are now in a position to focus on a subset of these seasonality hotspots—in northeast Brazil, western and central Africa, and northern Australia—and examine in more detail the changes over time in the magnitude, timing and duration of their seasonal rainfall regimes. To this end, a set of statistical measures are adopted for decomposing available station series. Specifically, the following indicators are used to quantify each of the seasonality components for each year: the annual rainfall (for the magnitude), the centroid of the monthly rainfall distribution (for the timing), and the spread (for the duration), which is a measure of the temporal deviation from the centroid of the monthly rainfall distribution (see Methods). The decomposition of the seasonal rainfall signal for a single station in Parau, Brazil (5.78° S, 37.1° W) into its indicator series is shown in Fig. 3.

For each indicator series (3 per station), we find its slope using linear or circular regression to assess temporal trends in the magnitude, timing and duration of seasonality (see Methods for dealing with gaps in data). Next, to find changes in its temporal variability, we compute the standard deviation of the residuals with a moving 12-year window (with windows of different lengths producing qualitatively similar results) and then find the slope of the resulting series by linear regression. The slopes for the trend and variability of each indicator series are assembled in box-plot forms in Fig. 4, and the significance of the mean deviation from no change in each region was evaluated with a Wilcoxon signed-rank test. The period of analysis is restricted to 1930–1990 owing to data availability.

The results show statistically significant changes in the trends (Fig. 4, top box plots) and increases in the variability of seasonality (Fig. 4, bottom box plots) throughout most of the dry tropics (see Supplementary Tables S2 and S3 for the mean and minimum/maximum indicator slope values for each region). Northeast Brazil, in particular, exhibits increases in the variability of seasonal magnitude and timing to a greater degree, on average, compared with other regions. This increased uncertainty associated

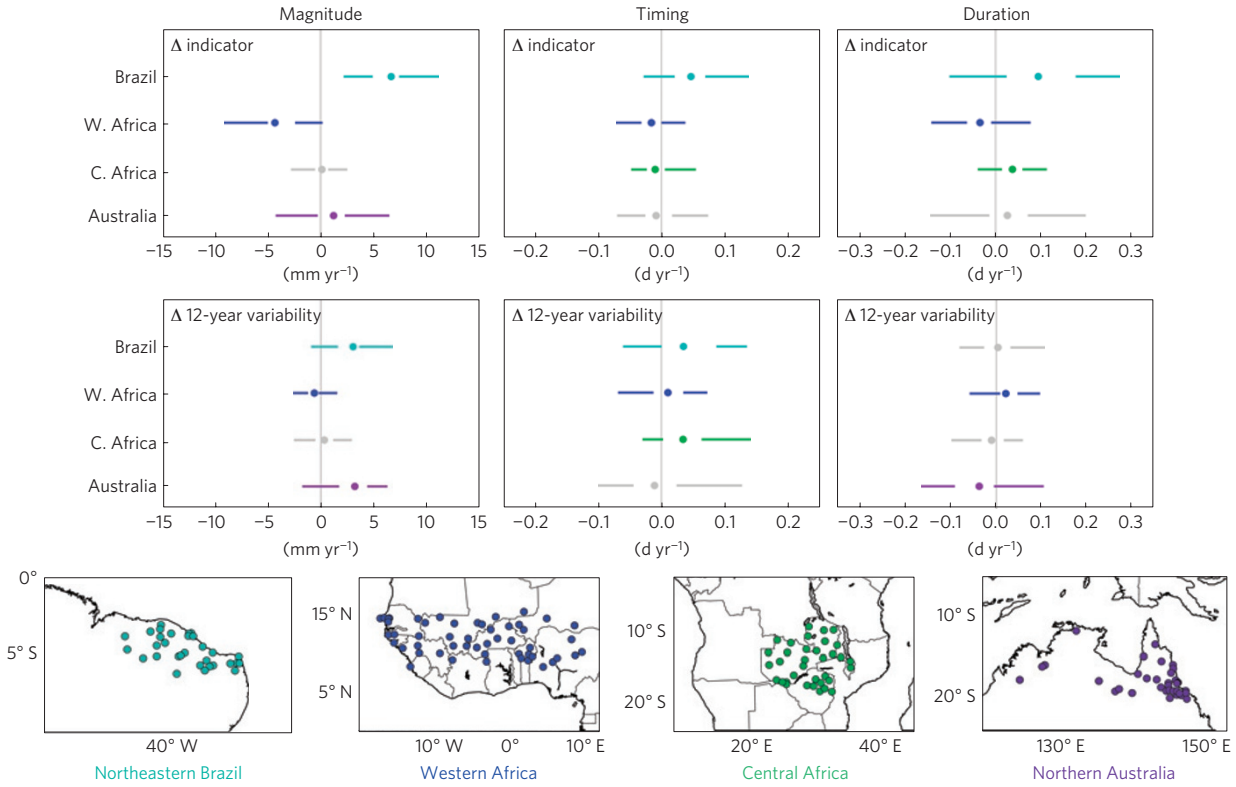

Figure 4 | Changes in rainfall magnitude, timing and duration in seasonality hotspots. The 6 box plots show ensembles for changes in the indicators for seasonal magnitude (annual rainfall; top left), timing (centroid; top middle) and duration (spread; top right), and changes in their 12-year variability (bottom row) from 1930 to 1990, using stations from the GHCN-Monthly data set (bottom maps). Data from northeast Brazil are in turquoise ($n = 30$), western Africa in blue ($n = 51$), central Africa in green ($n = 35$), and northern Australia in purple ($n = 38$). For each ensemble, the averages are indicated by a dot and the extent of the 25% and 75% percentiles by the whiskers. The ensembles for which the average values do not differ statistically from zero (using the Wilcoxon signed-rank test) are greyed.

with regional rainfall seasonality has occurred concurrently with increasing rainfall magnitude (average 6.7 [max 22] mm yr^{-1} (hereafter we abbreviate the listing of regional mean and extreme (either maximum or minimum) indicator slope values in the format of average (avg) [maximum/minimum])), delays in its timing (avg 0.045 [max 0.13] d yr^{-1}), and expansion of the wet season over 1930–1990. Western Africa generally shows trends in the opposite direction, with considerable decrease in the rainfall magnitude (avg −4.3 [min −18] mm yr^{-1}) and reduction in duration (avg −0.034 [min −0.14] d yr^{-1}) that have contributed to the previously detected decrease in seasonality (Fig. 2), whereas central Africa shows statistically significant increase in the variability of seasonal timing. The overall picture for parts of seasonal Africa is of a declining rainfall supply distributed over increasingly uncertain times. Northern Australia's increase in seasonality can be attributed to increase in the rainfall magnitude (avg 1.2 [max 6.4] mm yr^{-1}) with concomitant increase in duration (avg 0.026 [max 0.23] d yr^{-1}). Nevertheless, owing to the simultaneous increase in rainfall magnitude variability (avg 3.2 [max 11] mm yr^{-1}), the expected rainfall amount in each season has become more uncertain. These results are supported by a second complementary set of indicators based on demodulation[22,23] and information theory methods described in detail in the Supplementary Information.

To guide the interpretation of these results, we note that the slopes at a given station reflect long-term trends over the recorded period and thus should be summed over 60 years to determine their cumulative changes. We also verified that the trends produced from analysing the data at the monthly scale can indeed be interpreted at the daily scale, because these trends are almost equivalent to those analysed directly at the daily scale (Supplementary Figs S7 and S8 show the comparison for some stations where daily data are available). In addition, although the spatial means reveal broader regional tendencies, these tendencies are driven by more extreme changes occurring at individual stations, which are working synergistically to alter local landscapes. The increase in the uncertainty in the seasonal timings, as seen for example in parts of northeast Brazil and central Africa, may desynchronize phenology and other biological responses throughout several trophic levels in the ecosystem[8,14]. Likewise, the lengthening of the rainy season in northeast Brazil and central Africa may translate into an increase in the transpiration period[24] and shifts in the regional carbon budgets, and the decrease in seasonal rainfall seen in Africa may boost the competitive advantage of some plant functional types over others (for example, deciduous species at the expense of evergreen species[25]). For systems living near the margin of tolerance for available water, the occurrence of extremely wet or dry years can determine major compositional shifts as well as threshold responses such as mass tree mortality and disease outbreaks[26].

We project that this increased variability in conjunction with changing seasonality trends, if sustained into the next century, may portend significant shifts in the timing of plant activities[27] and ecosystem composition and distribution[10], with consequences for water and carbon cycling and water resource management in the tropics. To understand their full impacts, we must begin by detecting changes in all aspects of seasonality while recognizing their simultaneous contributions to informing the life strategies of individual species and to shaping overall ecosystem functioning. To that end, the framework introduced in this study can be broadly adopted for multi-dimensional analyses of seasonality, applicable not only to seasonally dry tropical regions, but also to Mediterranean and monsoonal climates where the annual rainfall is unevenly distributed. The results can then be used to inform on management strategies for mitigating water resource shortages and addressing ecosystem vulnerability in seasonally dry regions.

Methods

Seasonality index The monthly rainfall data from the Global Historical Climatology Network[19] (GHCN-Monthly; Supplementary Table S1) were downloaded from the IRI/LDEO Climate Data Library[28]. To construct the seasonality indices (equation (1)), stations with at least 20 years of data from 1970 to 1990 (including gaps) were selected (2,715 total) to obtain first their monthly rainfall climatology, calculated by averaging the monthly rainfall over all available years in each station. The hydrological year k is then defined starting on the first month after that of minimum mean rainfall and proceeds for 12 months, indexed by $m \in [1, 12]$. The monthly rainfall distribution is denoted for each hydrological year as $r_{k,m}$, and the monthly rainfall climatology is $\bar{r}_m = (1/k)\sum_k r_{k,m}$ averaged over all available years k.

The mean annual rainfall for each station is $\bar{R} = \sum_{m=1}^{12} \bar{r}_m$, and its monthly probability distribution is $\tilde{p}_m = \bar{r}_m/\bar{R}$. To present each station in the context of the global range, we normalize $\bar{R}$ by the maximum $\bar{R}$ of the entire GHCN-Monthly data set ($\bar{R}_{\max} = 7,932$ mm yr^{-1} in Tabubil, Papua New Guinea).

The relative entropy for each station, $\bar{D}$, can be calculated as $\bar{D} = \sum_{m=1}^{12} \tilde{p}_m \log_2(\tilde{p}_m/q_m)$, where q_m is the uniform distribution, for which each month has a value of 1/12. This is a positive semi-definite measure for the distance between the observed monthly rainfall distribution $\tilde{p}_m$ and the uniform distribution q_m. For our purposes, the relative entropy is a good description of the concentration of rainfall around the wet season and is then combined with $\bar{R}$ to define the long-term seasonality index as in equation (1).

The identification of seasonality hotspots using the GHCN-Monthly station data is corroborated by replicating the derivation of $\bar{S}$ using the CRU TS 2.1 gridded data set (Fig. 2), which has complete coverage from 1901 to 2002 over the tropics. Although the data at individual grid points are not suitable for seasonality decomposition owing to the extent of their spatial and temporal interpolation, it is nevertheless helpful to use this gridded data set for a first estimation of regions that are undergoing marked changes in seasonality. This is done by finding for each hydrologic year k its corresponding annual rainfall $R_k = \sum_{m=1}^{12} r_{k,m}$ (and associated distribution, $p_{k,m} = r_{k,m}/R_k$), relative entropy $D_k = \sum_{m=1}^{12} p_{k,m} \log_2(p_{k,m}/q_m)$, and seasonality index $S_k = D_k \cdot R_k/\bar{R}_{\max}$, and then applying linear regressions over their changes from 1930 to 2002. The slopes of the linear regression for the normalized R_k, D_k and S_k are shown in Supplementary Fig. S3.

Magnitude, timing and duration of seasonality. The rainfall seasonality hotspots from the GHCN-Monthly data set were visually identified as regions with high seasonality ($\bar{S}$) stations. Among those, we focused on northeastern Brazil, western and central Africa, and northern Australia for further analysis of specific seasonality components. To minimize the effect of missing data (see Supplementary Fig. S5 and Table S8), only stations with 2 or fewer consecutively missing monthly data between 1930 and 1990 were admitted for analysis from each region, reducing the total number of eligible stations to $n = 30$, 51, 35 and 38 for northeast Brazil, western Africa, central Africa and northern Australia, respectively. Missing data were then filled by linearly interpolating between the bounding months if they occur in the middle of the time series, or substituted with the corresponding mean monthly value if they occur at either ends. For every station, yearly indicator series for the magnitude, timing and duration of rainfall were obtained. For each hydrological year k, the annual rainfall (magnitude) is $R_k = \sum_{m=1}^{12} r_{k,m}$. The centroid C_k (timing) and the spread Z_k (duration) are found using the first and the second moments of $r_{k,m}$, specifically,

$$C_k = \frac{1}{R_k}\sum_{m=1}^{12} m r_{k,m}$$

$$Z_k = \sqrt{\frac{1}{R_k}\sum_{m=1}^{12} |m - C_k|^2 r_{k,m}}$$

A complementary set of indicators—the demodulated amplitude[22,23] (magnitude), the demodulated phase (timing) and the entropic spread (duration)—is described in the Supplementary Information.

Regional trends and variabilities. For all eligible rainfall series, regression was applied to each of the indicator series for the magnitude, timing and duration of seasonality. For the timing series (centroid and phase), circular-linear regression was performed with the circular package in R, and linear regression was performed on all other series using the scipy package in Python. Slopes from the regressions, for each indicator series in each region, were then assembled and presented in box-plot forms in Fig. 4, top row.

To find their variability over time, we passed a 12-year standard deviation moving window through the residuals of the series (circular standard deviation was used for phase and centroid). The slopes from the linear regression of all resulting variability series in each region were then similarly compiled into box-plot form and presented in Fig. 4, bottom row. The significance of the spatial ensembles was tested using the Wilcoxon signed-rank test, which compares against the null hypothesis that the mean value of the ensemble is zero. Those with p values greater than 0.05 were considered inconclusive (Supplementary Tables S4 and S7) and greyed on the plots.

Received 20 August 2012; accepted 18 April 2013; published online 19 May 2013

References

1. Easterling, D. R. Climate extremes: Observations, modeling, and impacts. *Science* **289,** 2068–2074 (2000).
2. Trenberth, K. E. *et al.* in *IPCC Climate Change 2007: The Physical Science Basis* (eds Solomon, S. *et al.*) Ch. 3 (Cambridge Univ. Press, 2007).
3. Zeng, N., Neelin, J., Lau, K. & Tucker, C. Enhancement of interdecadal climate variability in the sahel by vegetation interaction. *Science* **286,** 1537–1540 (1999).
4. Weltzin, J. F. *et al.* Assessing the response of terrestrial ecosystems to potential changes in precipitation. *BioScience* **53,** 941–952 (2003).
5. Austin, A. T. *et al.* Water pulses and biogeochemical cycles in arid and semiarid ecosystems. *Oecologia* **141,** 221–235 (2004).
6. Huxman, T. E. *et al.* Precipitation pulses and carbon fluxes in semiarid and arid ecosystems. *Oecologia* **141,** 254–68 (2004).
7. Briggs, J. M. & Knapp, A. K. Interannual variability in primary production in tallgrass prairie: Climate, soil moisture, topographic position, and fire as determinants of aboveground biomass. *Am. J. Bot.* **82,** 1024–1030 (1995).
8. Dirzo, R., Young, H. S., Mooney, H. A. & Ceballos, G. (eds) *Seasonally Dry Tropical Forests* (Island Press, 2011).
9. Singh, K. P. & Kushwaha, C. P. Emerging paradigms of tree phenology in dry tropics. *Curr. Sci.* **89,** 964–975 (2005).
10. Walther, G-R. *et al.* Ecological responses to recent climate change. *Nature* **416,** 389–395 (2002).
11. Wani, S. P., Rockstrom, J. & Oweis, T. Y. (eds) *Rainfed Agriculture?: Unlocking the Potential* (CAB International, 2009).
12. Borchert, R. Soil and stem water storage determine phenology and distribution of tropical dry forest trees. *Ecology* **75,** 1437–1449 (1994).
13. Eamus, D. Ecophysiological traits of deciduous and evergreen woody species in the seasonally dry tropics. *Trends Ecol. Evol.* **14,** 11–16 (1999).
14. Schwartz, M. D. (ed.) *Phenology: An Integrative Environmental Science* (Kluwer Academic, 2003).
15. Rockstrom, J., Barren, J. & Fox, P. in *Water Productivity in Agriculture: Limits and Opportunities for Improvement* (eds Kijne, J. W., Barker, R., & Molden, D. J.) 1127–1143 (CAB International, 2003).
16. Borchert, R. Climatic periodicity, phenology,and cambrium activity in tropical dry forest trees. *Iawa J.* **20,** 239–247 (1999).
17. Adejuwon, J. O. Rainfall seasonality in the Niger Delta Belt, Nigeria. *J. Geogr. Region. Plann.* **5,** 51–60 (2012).
18. Walsh, R. P. D. & Lawler, D. M. Rainfall seasonality: Description, spatial patterns and change through time. *Weather* **36,** 201–208 (1981).
19. Vose, R. S. *et al. The Global Historical Climatology Network: Long-term Monthly Temperature, Precipitation, Sea Level Pressure, and Station Pressure Data* (CDIAC, 1992).
20. Cover, T. M. & Thomas, J. A. *Elements of Information Theory* (John Wiley, 2006).
21. Mitchell, T. D. & Jones, P. D. An improved method of constructing a database of monthly climate observations and associated high-resolution grids. *Int. J. Climatol.* **25,** 693–712 (2005).
22. Rodriguez-Iturbe, I., Dawdy, D. R. & Garcia, L. E. Adequacy of Markovian models with cyclic components for stochastic streamflow simulation. *Wat. Resour. Res.* **7,** 1127–1143 (1971).
23. Bloomfield, P. *Fourier Analysis of Time Series: An Introduction* (John Wiley, 2000).
24. Yoshifuji, N. *et al.* Inter-annual variation in growing season length of a tropical seasonal forest in northern Thailand. *Forest Ecol. Manage.* **229,** 333–339 (2006).
25. Enquist, B. J. & Enquist, C. A. F. Long-term change within a Neotropical forest: Assessing differential functional and floristic responses to disturbance and drought. *Glob. Change Biol.* **17,** 1408–1424 (2011).
26. Allen, C. D. *et al.* A global overview of drought and heat-induced tree mortality reveals emerging climate change risks for forests. *Forest Ecol. Manage.* **259,** 660–684 (2010).
27. Cleland, E. E., Chuine, I., Menzel, A., Mooney, H. A. & Schwartz, M. D. Shifting plant phenology in response to global change. *Trends Ecol. Evol.* **22,** 357–365 (2007).
28. http://iridl.ldeo.columbia.edu/SOURCES/.NOAA/.NCDC/.GHCN/.v2beta/.

Acknowledgements

X.F. was supported by the US National Science Foundation (NSF) through the Graduate Research Fellowship Program. A.P. had support from the NSF through grant CBET-1033467, the US Department of Energy (DOE) through the Office of Biological and Environmental Research (BER) Terrestrial Carbon Processes (TCP) program (DE-SC0006967), the Agriculture and Food Research Initiative from the USDA National Institute of Food and Agriculture (2011-67003-30222), and the National Aeronautics and Space Administration (NASA) grant NNX09AN76G. I.R-I. acknowledges the support from NASA grant NNX08BA43A. We also thank P. Landolt and the Institute of Fazenda Tamandua in northeast Brazil for providing valuable insights during part of the study, and A. Nishimura for offering valuable suggestions for statistical analysis.

Author contributions

All authors conceived and designed the study. X.F. performed the analyses and wrote an initial draft of the paper, to which all authors contributed edits throughout. All authors helped to interpret the results.

Additional information

Supplementary information is available in the online version of the paper. Reprints and permissions information is available online at www.nature.com/reprints. Correspondence and requests for materials should be addressed to A.P.

Competing financial interests

The authors declare no competing financial interests.